Check for updates

Enhanced photocatalytic activity for degrading phenol in seawater by TiO$_2$-based catalysts under weak light irradiation†

Ting Wang, Zhi-yong Xu, Li-guang Wu, [iD]* Bing-rui Li, Mei-xi Chen, Shi-yi Xue, Yi-chen Zhu and Jing Cai

The seawater system is a typical salt water system. A catalyst should overcome the disturbance from the salt ions for an efficient photodegradation of organic pollutants in the seawater system. Commercial photocatalysts (P25) and La^{3+}-doped SiO$_2$–TiO$_2$ prepared using adsorbed-layer nanoreactor synthesis (ALNS) were first used for photodegrading different initial concentrations of phenol in seawater under weak UV light irradiation. The weak adsorption capacities for phenol and the hydrophilic surfaces of the two photocatalysts could not overcome the disturbance of salt ions and thus showed low photocatalytic activities. Based on this, graphene oxide (GO) was used as a support to prepare TiO$_2$ and La^{3+}-doped TiO$_2$ using ALNS. The solvothermal treatment with alcohol was used as a solvent for both TiO$_2$ crystallization and GO reduction. Results showed that TiO$_2$ nanoparticles with sizes <10 nm formed and distributed homogeneously on the reduced GO surface. The small size of the TiO$_2$ particles and the decreased oxygenated functional groups on the GO surface both caused high separation efficiency of the photogenerated charge carriers, thereby increasing the photodegradation performance. The strong phenol adsorption of the photocatalyst was efficient enough to overcome the interference of salt ions and enhance the photodegradation efficiency in seawater. The activities of the two Red–GO–TiO$_2$ catalysts were more than twice those of P25 and La^{3+}-doped SiO$_2$–TiO$_2$. La^{3+} doping caused mixed crystals to form and increased the shallow trapping sites for charge carriers. Therefore, La^{3+} doping increases the photocatalytic activity of Red–GO–TiO$_2$.

Introduction

The rapid development of industry has initiated numerous environmental pollution problems.[1,2] For example, the ocean is facing difficult organic pollution problems due to terrestrial

School of Environmental Science and Engineering, Zhejiang Gongshang University, Hangzhou, 310012, China. E-mail: wulg64@hotmail.com

† Electronic supplementary information (ESI) available: Dependences of conductivity of seawater on time after photocatalysts addition, dependences of conductivity of seawater on time after photocatalysts addition, the standard curve of phenol in seawater and water measured by spectrophotometer, the blank degradation experiments of phenol illuminated under 4 W UV lamp, degradation of phenol with different initial concentration by two catalysts in seawater, degradation of phenol with different initial concentration by two catalysts in water, digital photographs of the dispersion of La^{3+} doped SiO$_2$–TiO$_2$ in seawater, TEM images of Red–GO samples, TEM images of two GO–TiO$_2$ before solvothermal treatment, XPS profiles of Ti 2p in two Red–GO–TiO$_2$ catalysts, digital photographs of the dispersion of GO–TiO$_2$ and Red–GO–TiO$_2$ in seawater, HRTEM images of GO–TiO$_2$ before solvothermal treatment, photocurrent response of different photocatalysts, photodegradation of different phenol concentrations using GO–TiO$_2$, degradation curves using Red–GO–TiO$_2$ and degradation curves using La^{3+} doping Red–GO–TiO$_2$ are shown in Fig. S1–S16. The mechanism scheme on photodegradation process for phenol in seawater by Red–GO–TiO$_2$ with or without doping is shown in Scheme S1. See DOI: 10.1039/c7ra04732k

pollutant emissions and numerous sailing ships.[3,4] The marine system is first a typical salt water system (salt concentration is generally between 3–5%) that interferes with traditional treatment technologies, such as microbial degradation, for organic pollutants.[5,6] Second, the organic pollutant concentration in seawater is low; therefore, effective treatments using traditional adsorption technology are costly and difficult.[7] At present, few studies have focused on effectively eliminating organic pollutants from seawater. For decades, developing advanced oxidation technologies has provided new ideas for removing organic pollutants in the ocean.[8] TiO$_2$-based heterogeneous semiconductor photocatalysis is the most intensively studied technology for pollutant treatment among advanced oxidation technologies, because of its low energy consumption and pollution-free process.[9–11] Especially, heterogeneous photocatalysis shows excellent potential in degrading highly toxic organic pollutants with low concentration. In heterogeneous photocatalysis, small TiO$_2$ particles, especially the quantum-sized TiO$_2$ particles (less than 10 nm), show high activity.[12–14] However, small nanoparticles easily agglomerate during preparation and application to form large particles and reduce or even halt the catalytic activity. To mediate particle agglomeration, supported catalysts have been presented and prepared in

numerous studies.[15,16] Considering its enhanced light adsorption and separation of photogenerated carriers, SiO_2 and new carbon nanomaterials (carbon nanotubes and graphene) have the high potential as support materials.[17,18]

However, high-power light sources, such as high-pressure mercury that emit several hundred watts, were used in most studies as excitation light sources.[19,20] The intensities of these high-power light sources significantly exceed the strong natural sunlight environment with a light intensity of 1 W cm^{-2}.[21] In marine environments, light intensity is usually less than 1 mW cm^{-2}. Therefore, the strong-intensity light sources used in present studies limit the practical application of heterogeneous photocatalysis for eliminating organic pollutants from the ocean.[19,20] Fujishima first studied photocatalysis using a low-intensity light system and found that short carbon-chain alcohols and bacteria could be photodegraded using TiO_2 films under weak UV light irradiation.[22–24] Moreover, the quantum yield of photoreaction under weak UV light irradiation was visibly higher than that of the photodegradation excited by the strong UV light.[19] In our previous work,[25] TiO_2 with a quantum size of less than 7 nm and prepared using adsorbed-layer nanoreactor synthesis (ALNS) showed higher activity in photo-degrading methyl orange under weak light irradiation compared with P25 commercial photocatalyst. Given the formation of few photogenerated charge carriers excited by weak light irradiation, the structure–activity relationship of catalysts was more sensitive than that under strong light irradiation.

One challenging aspect still remains regarding the use of heterogeneous photocatalysis in seawater systems. Numerous salt ions often decrease photocatalytic activity or cause photocatalyst inactivation.[26–29] Based on studies and our previous work,[30,31] the photodegradation for phenol by P25 and La^{3+}-doped SiO_2–TiO_2 *via* ALNS in seawater under weak UV light irradiation was first accomplished; afterward, TiO_2 particles and La^{3+}-doped TiO_2 particles with graphene oxide (GO) as a support were prepared using ALNS. A solvothermal treatment with alcohol as the reducing agent was used for both TiO_2 crystallization and GO reduction to enhance the photocatalytic activity for phenol in seawater.

Experimental

Materials

Graphite powder (G, 8000 mesh) was purchased from the Reagent Chemical Manufacturing (Shanghai, China). H_2SO_4, $KMnO_4$, $NaNO_3$, and lanthanum nitrate La(NO$_3$)$_3$ were obtained from Shanghai Reagent Factory (Shanghai, China). Analytical grade tetrabutyl titanate was received from the Reagent Chemical Manufacturer (Shanghai, China) and was used without further purification. Analytical grade ethanol was purchased from Reagent Chemical Manufacture of Shanghai and was distilled and stored over 4 Å molecular sieves before use. Nonporous hydrophilic colloidal silica (SiO_2) A-200 (12 nm, 200 m^2 g^{-1}) and P25 (gas nanometer TiO_2, 21 nm, 50 m^2 g^{-1}) were obtained from Degussa, Germany.

Preparation of graphene oxide with hydrophilic groups

Graphene oxide (GO) nanosheets with hydrophilic groups were synthesized by oxidizing graphite powder based on the improved Hummers method.[32] In previous studies, GO nanosheets optimized the morphology and distribution in polymer matrices upon addition of 5.0 g graphite powder, 2.5 g NaNO$_3$, and 20 g KMnO$_4$ to the suspension during GO preparation. These optimized conditions were maintained in the present study for synthesizing GO nanosheets. The specific surface area of GO nanosheets was 52 m^2 g^{-1}.

Preparation of TiO$_2$-based multiphotocatalysts

The preparation of SiO$_2$–TiO$_2$ doped with La^{3+} by ALNS. The preparation process referred to our previous work.[25] After we sintered TiO_2–SiO_2 doped with 0.5 wt% La^{3+} at 900 °C for 5 h and added 1.5 mL water and 2.15 g tetrabutyl titanate during catalyst preparation, it achieved peak photocatalytic activity. Therefore, these conditions were used to synthesize the undoped or doped TiO_2 photocatalysts in this study.

The preparation of Red–GO–TiO$_2$ by ALNS. GO–TiO$_2$ was first prepared using ALNS, as with our SiO$_2$–TiO$_2$ preparation in our previous work,[25] except that we used GO with hydrophilic groups as a support.

0.5 g of GO with hydrophilic groups, 1.5 mL of water and 200 mL of absolute alcohol were placed in a triflask, while stirring at 30 °C. A water-rich adsorption layer formed gradually on GO surface, due to the selective adsorption capacity for water. After adsorption equilibrium (24 h), tetrabutyl titanate (2.25 g) dissolved in alcohol (50 mL) was added. And tetrabutyl titanate could diffuse into the adsorption layer and the hydrolysis reaction takes place.[25] After 5 h of reaction, the product was obtained by centrifugation–washing cycles conducted three times.

The as-prepared TiO_2–GO catalysts were dispersed in 150 mL absolute alcohol and placed in a Teflon-covered stainless steel autoclave (volume: 200 mL). The autoclave was then placed in a furnace for solvothermal treatment (temperature: 170 °C, time: 24 h). After several centrifugation–washing cycles, the photocatalysts were retrieved and designated as Red–GO–TiO$_2$.

The preparation of Red–GO–TiO$_2$ doped with La^{3+} preparation by ALNS. The preparation process was similar to that of SiO$_2$–TiO$_2$ doped with La^{3+}.[25]

0.5 g of GO with hydrophilic groups, 1.5 mL of water and 200 mL of absolute alcohol were placed in a triflask, while stirring at 30 °C. A water-rich adsorption layer formed gradually on GO surface, due to the selective adsorption capacity for water. After adsorption equilibrium (24 h), tetrabutyl titanate (2.25 g) and lanthanum nitrate (0.77 mg) dissolved in alcohol (50 mL) was added. Both tetrabutyl titanate and La^{3+} ions could diffuse into the adsorption layer and the hydrolysis reaction takes place.[25] After 5 h of reaction, the product was obtained by centrifugation–washing cycles conducted three times.

The process of solvothermal treatment for this catalyst was similar as that of Red–GO–TiO$_2$. After the solvothermal treatment, the photocatalysts were retrieved and designated as La^{3+}-doped Red–GO–TiO$_2$.

Characterization

The morphologies of TiO_2–GO catalysts were characterized using transmission electron microscopy (TEM, JEM-1230, Jeol Co., Ltd.). The Autosorb 1-C sorption system (Quantachrome, USA) was used to determine the specific surface area. The structure of TiO_2–GO catalysts was determined using Fourier transform infrared (FTIR) spectroscopy (Nexus-670, Nicolet Co.). Moreover, the catalysts were analyzed with X-ray diffraction (XRD) using a D/max-rA XRD instrument (XD-98) with Cu Kα radiation (1.5406 Å). The photoluminescence (PL) spectra were recorded on a fluorospectrophotometer (PL: RAMANLOG 6, USA) at room temperature using a 250 nm xenon lamp as the irradiation source. The surface properties of catalysts were investigated using X-ray photoelectron spectroscopy (XPS) with Al Kα X-ray (hm = 1486.6 eV) radiation operated at 150 W (XPS: Thermo ESCALAB 250, USA).

Photocatalysis experiments

Our experiment used simulated seawater composed of 2.5% NaCl, 1.1% $MgCl_2$, 0.40% Na_2SO_4, and 0.16% $CaCl_2$ in distilled water without CO_2.[33,34] Conductivity measurements were used to evaluate the effects of photocatalyst addition on seawater salt concentration. As shown in Fig. S1 and S2 in the ESI,† the solution conductivity did not change after photocatalyst addition. It is suggested that the adsorption amount of salt ions by these photocatalysts in seawater was too small to be measured by the conductivity measurements.

The photodegradation of phenol in seawater was studied to evaluate the performance of different catalysts irradiated under weak ultraviolet (UV) black-light lamps (250 nm wavelength, 4 W).[25] Prior to irradiation, the suspension (800 mL of phenol solution with different initial concentration, 1.0 g of different photocatalysts) was stirred in the dark for 60 min to establish a adsorption/desorption equilibrium. At 30 min intervals, the sampled suspension was centrifuged, and the upper clear solution was extracted. UV-vis spectrophotometer (Beijing, China) was used to measure the changes in the phenol concentration (510 nm wavelength) in the solution using the 4-aminoantipyrine spectrophotometric method (Fig. S3, ESI†). To confirm the results from the 4-aminoantipyrine spectrophotometric method,[35,36] we determined the total organic carbon (TOC) in the aqueous solution without catalysts after 5 h of photodegradation. And it was found that the removal rate of phenol by TOC was approximated by the results of spectrophotometry, which meant phenol in seawater transfer to form CO_2 and H_2O after 5 h of photodegradation.

Fig. S4 (ESI†) provides the details on the blank experiments under weak UV light irradiation with an intensity of 12 μW cm^{-2}. The light intensity of the four-watt UV lamp was weak for degrading phenol.

Results and discussion

Comparison of photodegradation in seawater and in water excited by weak UV light

The photodegradation of different phenol concentrations in seawater using P25 and SiO_2–TiO_2 doped with La^{3+} was first investigated. The photodegradation experiments in water using the same catalysts were done simultaneously for comparison. The photodegradation curves of phenol in seawater and water are listed in Fig. 1 and 2, respectively.

The curves in Fig. 1 and 2 shows that all catalysts reach adsorption equilibrium for phenol both in seawater and water after 30 min. Two catalysts had poor adsorption for phenol in seawater or water, due to their hydrophilic surfaces. Under weak UV light irradiation, the degradation for phenol by the two catalysts in seawater and water almost followed a first-order reaction kinetics, which agreed with previous results.[37,38] Under same conditions, SiO_2–TiO_2 doped with La^{3+} had higher photocatalytic activity than P25 under weak UV light irradiation, which corresponded with our previous results.[25] According to heterogeneous photocatalysis studies, the amount of catalyst surface active center was limited. At a high initial concentration, a large amount of phenol molecules could not efficiently be photodegraded by catalysts. The catalyst activity was reduced and the degradation process was deviated from a first-order reaction kinetics.
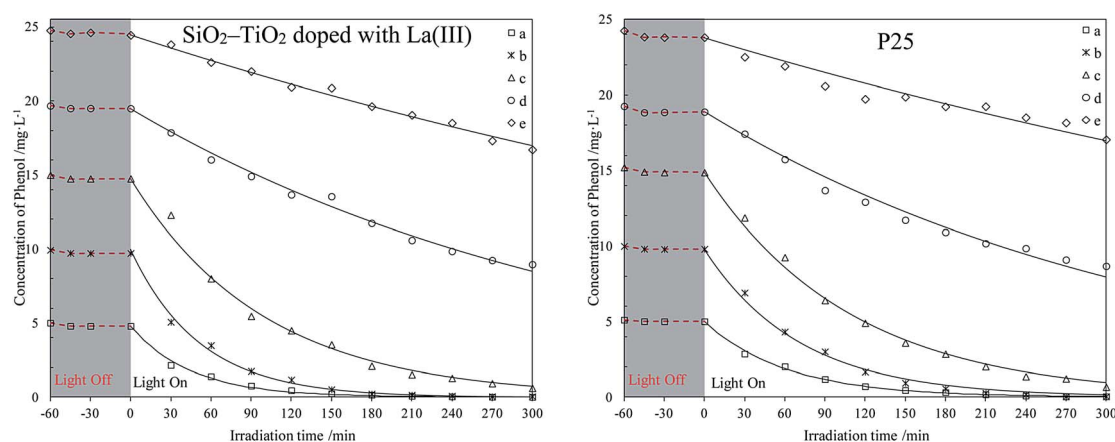

Fig. 1 Photodegradation of different phenol concentrations in seawater using two catalysts. The initial phenol concentrations (mg L^{-1}): (a) 5; (b) 10; (c) 15; (d) 20; (e) 25.
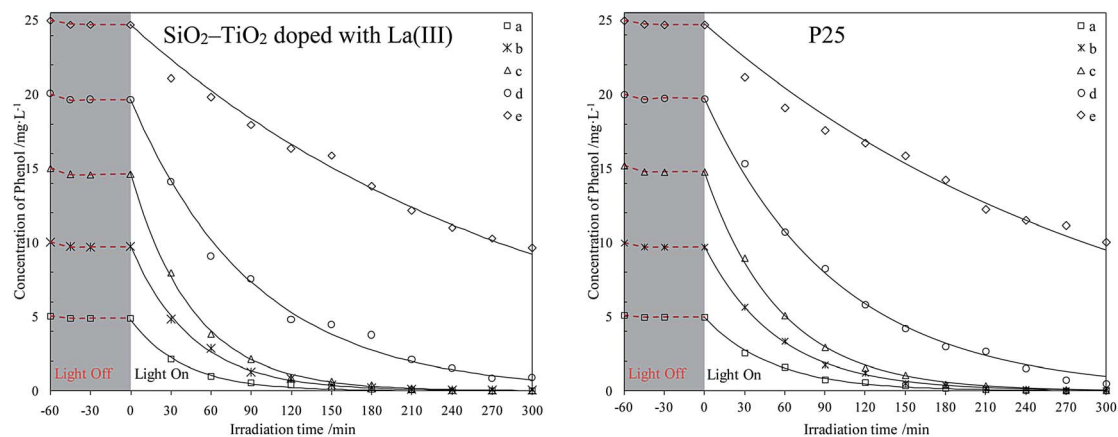
Fig. 2 Photodegradation of different phenol concentrations in water using two catalysts. The initial phenol concentrations (mg L^{-1}): (a) 5; (b) 10; (c) 15; (d) 20; (e) 25.
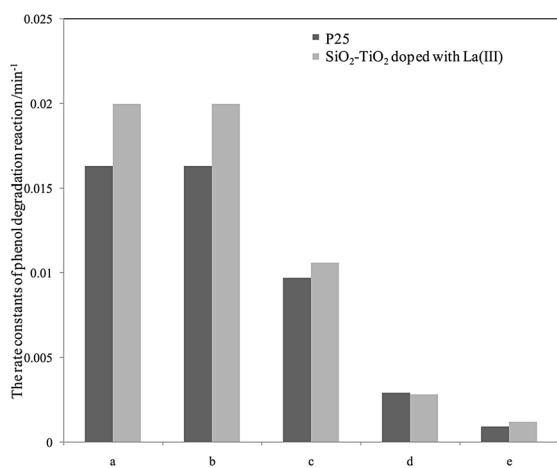
Fig. 3 Dependence of initial phenol concentration on the photo-degradation rate constants using two catalysts in seawater. The initial phenol concentrations (mg L^{-1}): (a) 5; (b) 10; (c) 15; (d) 20; (e) 25.

decreased obviously, whereas in water, the activities of the two catalysts were reduced at a high initial phenol concentration (≥ 20 mg L^{-1}).

Based on the comparison of the results in seawater and in water, the catalyst must meet two requirements to efficiently degrade organic matter in seawater systems. Firstly, the TiO$_2$ photocatalysts should have the necessary microstructures, such as small particle size, high dispersibility, and appropriate crystal form, in the photodegradation process in water. On the other hand, the previous results[25] indicated that weakening the surface hydrophilicity of the catalyst and increasing the adsorption performance of the catalyst for target organics in seawater are also necessary. Based on current and previous results,[26,27] we first employed solvothermal treatment using ethanol as a reduction solvent to change the surface properties of the SiO$_2$–TiO$_2$ catalyst. Fig. S7 (ESI†) shows the digital photos of the SiO$_2$–TiO$_2$ catalyst before and after the solvothermal treatment in seawater. The surface hydrophilicity of the SiO$_2$–TiO$_2$ catalyst after the solvothermal treatment was significantly

Comparing all photodegradation curves in Fig. 1 and 2, the changes in photodegradation in seawater and water vary as the phenol concentration increases. Under the same condition, the same catalyst had lower activity in seawater than in water. In seawater, the salt ions were much more than the phenol molecules. Combining the results in studies,[39–41] large amount of salt ions would move around the catalyst surface, due to the hydrophilic surface of P25 or SiO$_2$–TiO$_2$ doped with La^{3+}. This inhibited the phenol diffusion from the bulk to the catalyst surface and decreased the catalyst activity center.

For further comparison, the rate constants in seawater and water were obtained by plotting ln(C_0/C) to irradiation time t (as shown in Fig. S5 and S6, ESI†) and are listed in Fig. 3 and 4. The changes in the two figures indicate that the activities of two catalysts in seawater were lower than those in water under the same conditions, due to the presence of so many salt ions. In seawater, the catalyst activity was more sensitive to the initial concentration of phenol than that in water. At the initial concentration of 15 mg L^{-1}, the activities of the two catalysts
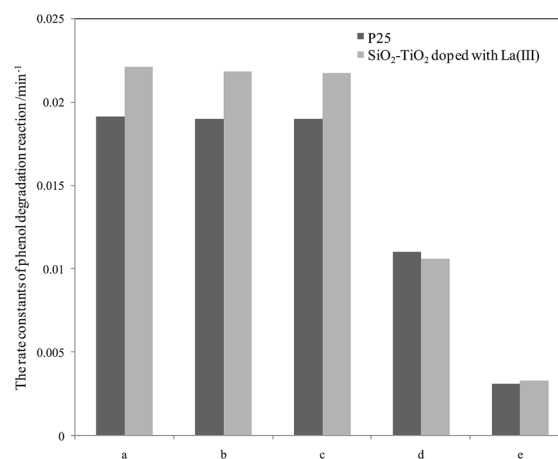

Fig. 4 Dependence of initial phenol concentration on the photo-degradation rate constants using two catalysts in water. The initial phenol concentrations (mg L^{-1}): (a) 5; (b) 10; (c) 15; (d) 20; (e) 25.
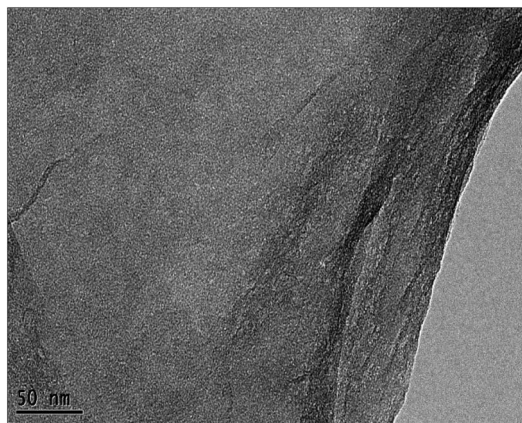
Fig. 5 TEM image of GO nanosheets as a support.

weakened. However, the SiO_2–TiO_2 catalyst after the solvothermal treatment was unable to disperse uniformly in water, therefore, photodegradation could not be done. Combining our former results[25,30] and those of others,[26,27] we first used GO with a hydrophilic surface as a support in preparing small TiO_2 particles using ALNS. The solvothermal treatment was used to reduce the oxidation groups on the catalyst surface, aiming to decrease the surface hydrophilicity and increase the adsorption of the catalyst for organics in seawater. The TEM image of the GO nanosheets is shown in Fig. 5.

Preparation of different Red–GO–TiO₂ by coupling ALNS and solvothermal treatment

From Fig. 5, the highly transparent nanosheets with yarn-like sheets are characteristic of the GO morphology, which indicate a monolayer or a few layers of GO. These findings are consistent with previous work.[32] Fig. 6 lists the adsorption curves of water by GO and the adsorption equilibrium after 4 h (240 min). Assuming that the adsorption layer is entirely composed of water, the adsorption layer thickness of GO is approximately 1 nm, thereby proving that the water-rich adsorption layer will form on the GO surface. Thus, this
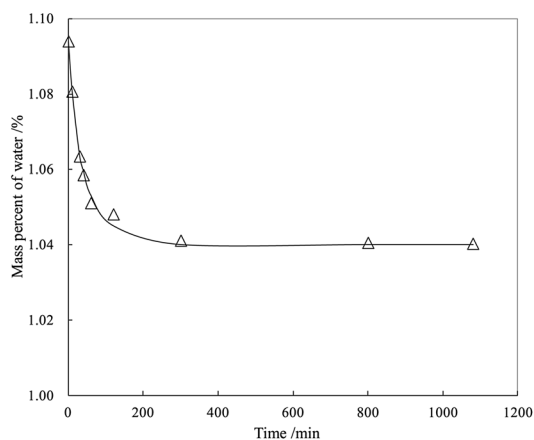

Fig. 6 Dependences of water adsorbed by GO on adsorption time.

adsorption layer can be used as a nanoreactor for preparing TiO_2 nanoparticles.

For a clear comparison, GO sample was denoted as Red–GO after the solvothermal treatment, and its TEM image is listed in Fig. S8 (ESI†). As shown in the figure, TEM morphologies of both GO and Red–GO nanosheets showed a yarn-like sheet structure, indicating that the solvothermal treatment did not change the nanosheet morphology. The specific surface area of Red–GO nanosheets was 55 m^2 g^{-1}, similar to that of the GO nanosheets, which confirmed that the nanosheet morphology was unchanged by the solvothermal treatment.

Fig. 7 displays the TEM images of Red–GO–TiO_2 and La^{3+}-doped Red–GO–TiO_2, whereas Fig. S9 (ESI†) presents those of GO–TiO_2 and La^{3+}-doped GO–TiO_2 before solvothermal treatment for comparison. Manifested as the black points on the nanosheets, the TiO_2 particle morphology can be observed both in Fig. 7 and S9 (ESI†).

The ALNS method employed a water-rich adsorption layer with several nanometer thick as a nanoreactor on the GO surface; therefore, TiO_2 nanoparticles with size of less than 10 nm were formed and were distributed homogeneously on the GO surface, as shown in Fig. S9 (ESI†). La^{3+} doping did not change the TiO_2 morphology on the GO surface, corresponding with previous findings.[25] Moreover, TiO_2 small particles that formed in the adsorption layer interacted tightly with the GO surface, and this could effectively inhibit the aggregation of both small TiO_2 particles and GO nanosheets during the solvothermal treatment. Therefore, no difference was observed in the catalyst morphology before and after the solvothermal treatment. The specific surface areas of Red–GO–TiO_2 and La^{3+}-doped Red–GO–TiO_2 were 51 and 50 m^2 g^{-1}, respectively, which were close to that of GO.

Fig. 8 displays the XPS results for different catalysts and suggests TiO_2 formation in all photocatalysts by ALNS. XPS analysis was used to identify the chemical state of Ti in the Red–GO–TiO_2 and La^{3+}-doped Red–GO–TiO_2 catalysts, as shown in Fig. S10 (ESI†). The Ti 2p levels of all catalysts depicted two peaks at approximately 464.6 and 458.3 eV, which were denoted as Ti $2p_{1/2}$ and Ti $2p_{3/2}$, respectively.[42] Data suggested that Ti existed as Ti^{4+} in the Red–GO–TiO_2 and La^{3+}-doped Red–GO–TiO_2 catalysts.

The solvothermal treatment had little influence on the catalyst morphology. However, the FTIR spectra of different photocatalysts (Fig. 9) indicated that the surface properties of the catalysts changed significantly after the solvothermal treatment. As shown in Fig. 9, GO–TiO_2 had a similar characteristic FTIR spectra with GO. The absorption bands corresponded to the C–O stretching at 1050 cm^{-1}, C–O–C stretching at 1250 cm^{-1}, C–OH stretching at 1400 cm^{-1}, C–C stretching at 1620 cm^{-1}, and C=O carbonyl stretching at 1720 cm^{-1}.[43] The resonance peak at 3383 cm^{-1} was assigned to the absorbed hydroxyl groups in catalysts.[44] When TiO_2 formed on the GO surface through ALNS, the TiO_2–GO catalysts exhibited weak absorption peaks of C–O, C–OH, C=O, and absorbed hydroxyl groups, thereby indicating that the oxygenated functional groups on GO surface slightly decreased during the formation of TiO_2 particles.
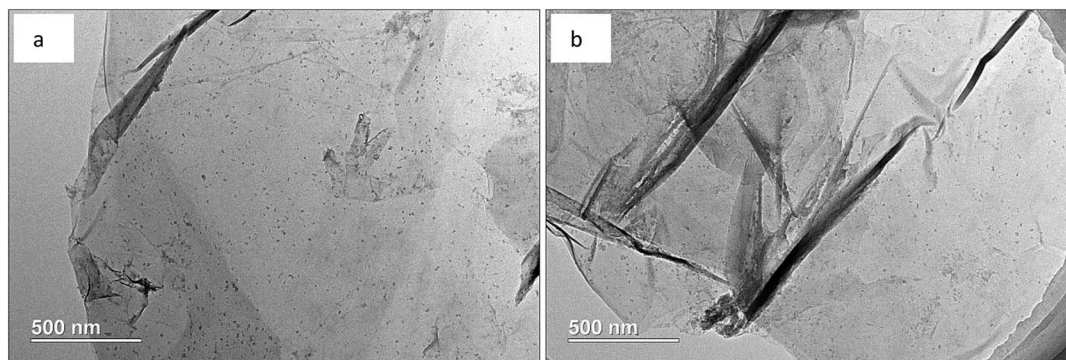
Fig. 7 TEM images of different Red–GO catalysts (a) Red–GO–TiO$_2$; (b) La^{3+}-doped Red–GO–TiO$_2$.
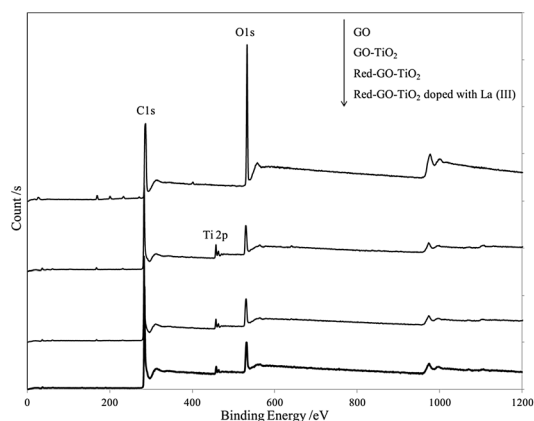

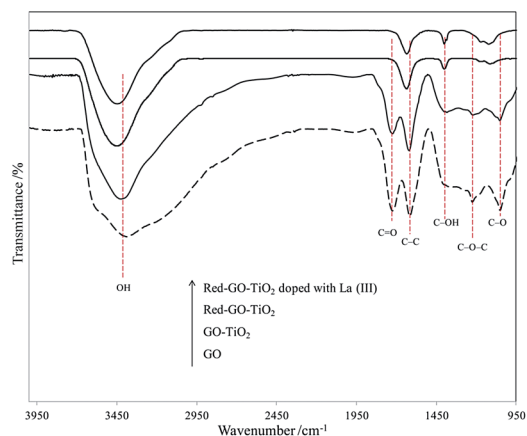**Fig. 8** XPS profiles of GO and different photocatalysts.

Fig. 9 FTIR spectra of GO and different photocatalysts.

After solvothermal treatment, the oxygenated functional groups on the surface of Red–GO–TiO$_2$ and La^{3+}-doped Red–GO–TiO$_2$ were reduced significantly and the absorption peaks of C=O and C–O–C almost disappeared. The GO surface was reduced during the solvothermal treatment with alcohol as the reducing agent, thereby confirming that alcohol reduced the oxygenated functional groups on the catalyst surface. The FTIR spectra of Red–GO–TiO$_2$ and La^{3+}-doped Red–GO–TiO$_2$ showed some remaining hydroxyl groups on the two catalyst surfaces, which would mainly be distributed on the TiO$_2$ surface. This could help in the efficient distribution of Red–GO–TiO$_2$ and La^{3+}-doped Red–GO–TiO$_2$ in seawater (as shown in Fig. S11†).

HRTEM results (Fig. 10) show that TiO$_2$ crystallization was simultaneous with the GO surface reduction during the solvothermal treatment. The HRTEM image of GO–TiO$_2$ is listed in Fig. S12 (ESI†) for comparison.

In the HRTEM image of GO–TiO$_2$ and the images in Fig. 10, the TiO$_2$ crystallization formed in both Red–GO–TiO$_2$ and La^{3+}-doped Red–GO–TiO$_2$ after the solvothermal treatment. These two catalysts had TiO$_2$ nanocrystals with less than 5 nm in size due to the small nanoreactors and Red–GO protection on TiO$_2$ particles. Several distortions were observed in the lattice fringes of the TiO$_2$ nanocrystals in the two catalysts, especially in the La^{3+}-doped Red–GO–TiO$_2$. Based on the results both in Fig. 7 and in our previous study,[25] the tight interaction between TiO$_2$ particles and the supports, as well as La^{3+} doping, caused the lattice distortions of TiO$_2$ during TiO$_2$ crystallization.

The XRD results in Fig. 11 confirm the formation of TiO$_2$ crystallization and the difference in TiO$_2$ crystallization between the two catalysts.

Fig. 11 shows that GO–TiO$_2$ has a similar XRD pattern with GO, and no TiO$_2$ crystallization peaks are present in the XRD pattern; therefore, the TiO$_2$ in GO–TiO$_2$ existed as amorphous TiO$_2$. After the solvothermal treatment, amorphous TiO$_2$ transformed into anatase TiO$_2$ crystals in Red–GO–TiO$_2$. Moreover, a few rutile TiO$_2$ crystals appeared in the La^{3+}-doped Red–GO–TiO$_2$, although anatase TiO$_2$ was the main crystal form. This phenomenon was not found in our previous works[25,30,31] and might be due to the strong inhibition by SiO$_2$ on TiO$_2$ crystallization than that of GO. In our previous work,[25] SiO$_2$ strongly inhibited the crystallization transformation of TiO$_2$, and the anatase TiO$_2$ did not transfer to rutile TiO$_2$ even with sintering at 900 °C. Therefore, a low level of La ion doping did not change the crystallization transformation of TiO$_2$. Due to the weak effect of GO on the crystallization transformation of TiO$_2$, a low level of La ion doping could improve the transformation of anatase TiO$_2$ to rutile TiO$_2$, which could cause the lattice distortions in the TiO$_2$ crystallization.[25,45]
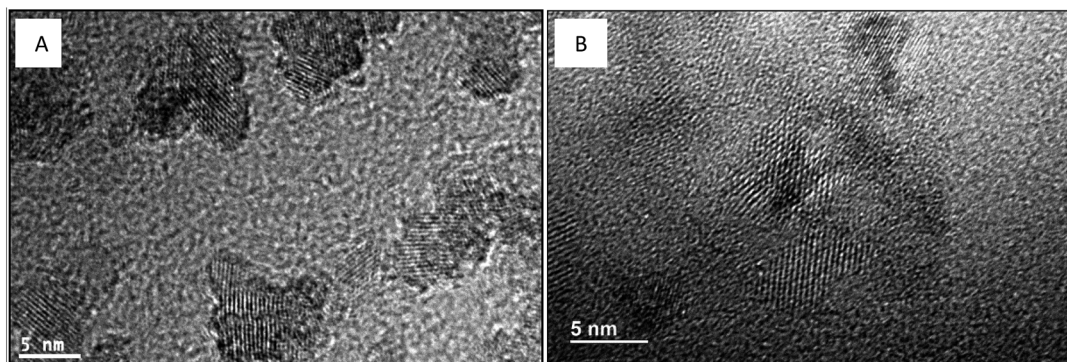
Fig. 10 TEM and HRTEM images of different TiO_2–RGO catalysts. (A) Red–GO–TiO_2; (B) GO–TiO_2 doped with La^{3+}.
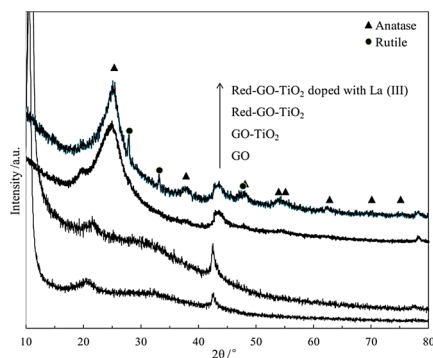

Fig. 11 XRD patterns of GO and different photocatalysts.

The changes in the surface property and TiO_2 crystallization would certainly affect the photocatalytic process. A low recombination rate of photogenerated electron–hole pairs result in high catalytic activity that could be attributed to the separation efficiency of photogenerated charge carriers and small intensities of PL peaks.[46]

Fig. 12 shows the differences in the PL spectra of GO, GO–TiO_2, Red–GO–TiO_2, and La^{3+}-doped Red–GO–TiO_2. Oxygenated functional groups on the GO surface could work as deep trapping sites for photogenerated charge carriers. Thus, GO and GO–TiO_2 showed similar PL peaks with strong intensities. After the solvothermal treatment, the oxygenated functional groups
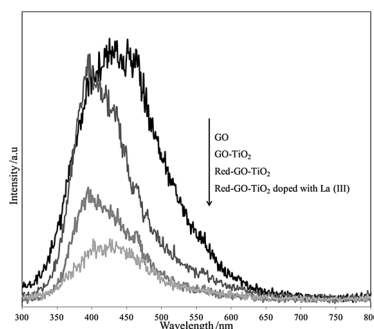

Fig. 12 PL spectra of GO and different photocatalysts with 250 nm excitation wavelength.

were reduced by alcohol and Red–GO could transport photogenerated electrons,[47,48] thereby weakening the PL peaks. The PL spectra also show that the photogenerated charge carrier was transferred rapidly from the TiO_2 particles to the Red–GO nanosheets, since the small TiO_2 particles tightly attached to the Red–GO surface in the two Red–GO–TiO_2 catalysts. This could significantly enhance the separation efficiency of photogenerated charge carriers and weaken the PL peak intensity. Moreover, a few lattice distortions in TiO_2 nanocrystals could work as shallow trapping sites for charge carriers. Especially, the mixed crystal forms, including anatase and rutile TiO_2, could introduce numerous shallow trapping sites as charge carriers into the catalysts. Therefore, the La^{3+}-doped Red–GO–TiO_2 had the weakest PL peak among the PL spectra in Fig. 12.

The photocurrent response of different catalysts could confirm further the results in PL test, as shown in Fig. S13 (ESI†). From the figure, it can be found that GO–TiO_2 has very weak photocurrent, due to oxygenated functional groups on the GO surface and amorphous TiO_2. The value of Red–GO–TiO_2 and La^{3+} doping Red–GO–TiO_2 were significantly higher than that of GO–TiO_2, since the oxygenated functional groups were reduced by alcohol and TiO_2 crystallization formed. La^{3+} doping introduced a few lattice distortions in TiO_2 nanocrystals as shallow trapping sites, so it had the strongest photocurrent response.

Performance of different Red–GO–TiO_2 by coupling ALNS and solvothermal treatment

The photodegradation experiments for phenol with different initial concentration of GO–TiO_2 were carried out. And the degradation curves are listed in Fig. S14.† Both amorphous TiO_2 and large amount of oxygenated functional groups on the GO surface worked as deep trapping sites for photogenerated charge carriers. Therefore, the GO–TiO_2 showed very low photocatalytic activity for phenol in seawater, under irradiation of weak UV light. In addition, the adsorption capacity of phenol by GO was also weak due to the hydrophilicity of GO surface.

Fig. 13 and 14 display the photodegradation of different phenol concentrations using Red–GO–TiO_2 and La^{3+}-doped Red–GO–TiO_2. From these curves, the two Red–GO–TiO_2 catalysts are shown to have strong adsorption capacity for phenol in seawater after the solvothermal treatment. We also list the C/C_0
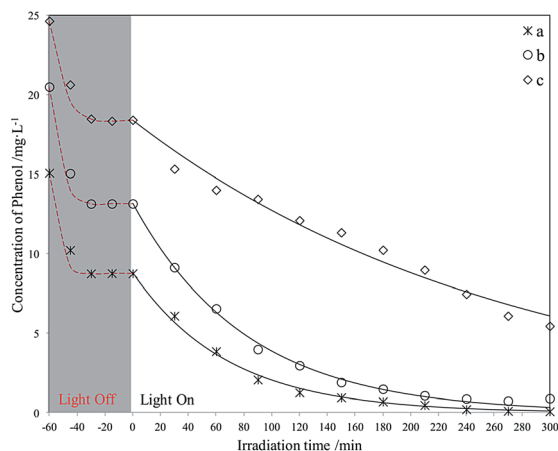
Fig. 13 Photodegradation of different phenol concentrations using Red−GO−TiO$_2$. The initial phenol concentration in seawater (mg L^{-1}): (a) 15; (b) 20; (c) 25.
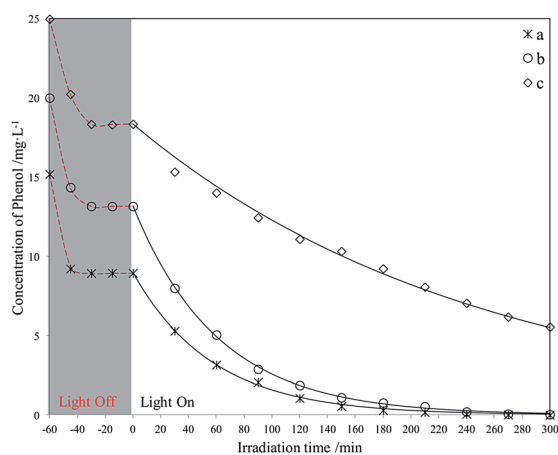

Fig. 14 Photodegradation of different phenol concentrations using La^{3+}-doped Red−GO−TiO$_2$. The initial phenol concentration in seawater (mg L^{-1}): (a) 15; (b) 20; (c) 25.
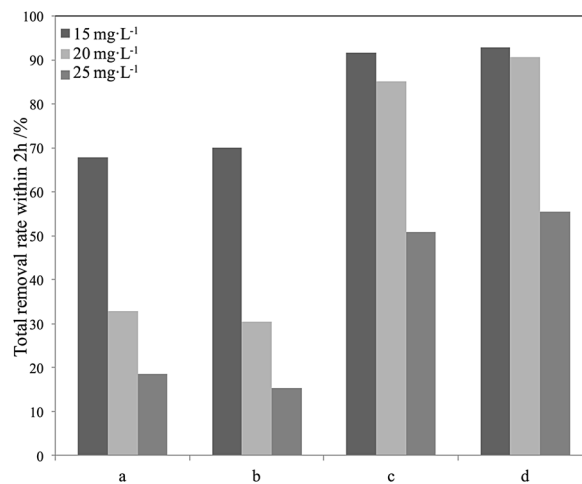

Fig. 15 Degradation efficiency of different phenol concentrations using different photocatalysts in seawater within 2 h (a) P25; (b) La^{3+}-doped SiO$_2$−TiO$_2$; (c) Red−GO−TiO$_2$; (d) La^{3+}-doped Red−GO−TiO$_2$.

graphs where C_0 is the concentration at the time that the light is switched on, as shown in Fig. S15 and S16.† As shown in all degradation curves, the photocatalytic activities of the two catalysts exceeded those of P25 and SiO$_2$−TiO$_2$ doped with La^{3+}, especially at high initial concentrations ($\geq$20 mg L^{-1}). The total phenol removal rates at 2 h using different photocatalysts are listed in Fig. 15.

As shown in Fig. 15, both Red−GO−TiO$_2$ and La^{3+}-doped Red−GO−TiO$_2$ had significantly higher activities than P25 and La^{3+}-doped SiO$_2$−TiO$_2$ at high initial phenol concentrations. The total removal rate of the two Red−GO−TiO$_2$ catalysts within 2 h was more than twice those of P25 and La^{3+}-doped SiO$_2$−TiO$_2$. This is mainly caused by both strong adsorption capability for phenol in seawater and the rapid transformation of photogenerated electrons from TiO$_2$ to Red−GO, as shown in Scheme S1 (ESI†).[49]

Comparing Red−GO−TiO$_2$ with or without doping, the two catalysts had similar adsorption capacities for phenol in

seawater. The La^{3+}-doped Red−GO−TiO$_2$ showed higher activity than Red−GO−TiO$_2$ without doping. From the HRTEM and XRD analyses in Fig. 8 and 9, La^{3+} doping caused mixed crystals to form, including anatase and rutile TiO$_2$, which could increase the shallow trapping sites in the catalysts for charge carriers. Thus, the photocatalytic activity of Red−GO−TiO$_2$ increased after La^{3+} doping. However, the enhancement on the activity was small, which was inconsistent with our previous studies. And this results suggested that the strong adsorption capability for phenol and the rapid transformation of photogenerated electrons played the more important roles on the enhancement on the photo activity in seawater than that of La^{3+} doping. This might be due to the difference between the catalysts prepared with GO as the carrier and the catalysts prepared with SiO$_2$ as the carrier. These require further studies.

Conclusions

Due to the weak phenol adsorption and hydrophilic surface, P25 and La^{3+}-doped SiO$_2$−TiO$_2$ could not overcome the disturbance of salt ions using ALNS. Therefore, they showed low activity in photodegrading phenol in seawater under weak UV light irradiation, especially at high initial phenol concentrations. Using ALNS coupling with solvothermal treatment with alcohol as the reducing agent, TiO$_2$ crystallization and RGO formation occurred simultaneously. The tight interaction between TiO$_2$ particles and the GO surface effectively inhibited TiO$_2$ aggregation during solvothermal treatment. Given the small size and efficient distribution of TiO$_2$ nanoparticles, the two Red−GO−TiO$_2$ catalysts showed high separation efficiency for photogenerated charge carriers. Moreover, the strong phenol adsorption on the two Red−GO−TiO$_2$ catalysts was essential for improving the photodegradation efficiency in seawater. The activities of the two Red−GO−TiO$_2$ catalysts were more than twice those of P25 and La^{3+}-doped SiO$_2$−TiO$_2$. Moreover, La^{3+} doping caused mixed crystals to form, including anatase and

rutile TiO_2, which could increase the shallow trapping sites in the catalysts for charge carriers. Thus, La^{3+} doping increases the photocatalytic activity of Red–GO–TiO_2.

Acknowledgements

Notes and references

1 N. P. Votsi, A. S. Kallimanis and I. D. Pantis, *Environ. Pollut.*, 2017, **221**, 459–469.

2 Y. Y. Wu, B. J. Gu, J. W. Erisman, S. Reis, Y. Y. Fang, X. H. Lu and X. M. Zhang, *Environ. Pollut.*, 2016, **218**, 86–94.

3 L. M. Rios, C. Moore and P. R Jones, *Mar. Pollut. Bull.*, 2007, **54**, 1230–1237.

4 R. Lohmann and I. M. Belkin, *Prog. Oceanogr.*, 2014, **128**, 172–184.

5 F. Kargi and A. R. Dincer, *Enzyme Microb. Technol.*, 1996, **19**, 529–537.

6 K. Windey, B. De and W. Verstraete, *Water Res.*, 2005, **39**, 4512–4520.

7 C. P. Huang, H. W. Wang and P. C. Chiu, *Water Res.*, 1998, **32**, 2257–2264.

8 M. Cheng, G. M. Zeng, D. L. Huang, C. Lai, P. Xu, C. Zhang and Y. Liu, *Chem. Eng. J.*, 2016, **284**, 582–598.

9 Y. A. Shabana, A. A. El Maradny and R. K. Al Farawati, *J. Photochem. Photobiol., A*, 2016, **328**, 114–121.

10 M. A. Lazar and W. A. Daoud, *RSC Adv.*, 2013, **3**, 4130–4140.

11 K. Fischer, M. Kühnert, R. Gläser and A. Schulze, *RSC Adv.*, 2015, **5**, 16340–16348.

12 P. V. Kamat and D. Meisel, *Curr. Opin. Colloid Interface Sci.*, 2002, **7**, 282–287.

13 C. L. Pang, R. Lindsay and G. Thornton, *Chem. Rev.*, 2013, **113**, 3887–3948.

14 H. H. Chen, C. E. Nanayakkara and V. H. Grassian, *Chem. Rev.*, 2012, **112**, 5919–5948.

15 D. Rubioa, J. F. Casanueva and E. Nebot, *J. Photochem. Photobiol., A*, 2013, **271**, 16–23.

16 X. H. Xia, Z. J. Jia, Y. Yu, Y. Liang, Z. Wang and L. L. Ma, *Carbon*, 2007, **45**, 717–721.

17 X. Jiang and T. Wang, *J. Am. Ceram. Soc.*, 2008, **91**, 46–50.

18 L. Gu, J. Y. Wang, H. Cheng, Y. Z. Zhao, L. F. Liu and X. J. Han, *ACS Appl. Mater. Interfaces*, 2013, **5**, 3085–3093.

19 M. R. Hoffmann, S. T. Martin, W. Y. Choi and D. W. Bahnemann, *Chem. Rev.*, 1995, **95**, 69–96.

20 W. Li, Y. Bai, C. Liu, Z. H. Yang, X. Feng, X. H. Lu, N. K. van der Laak and K. Y. Chan, *Environ. Sci. Technol.*, 2009, **43**, 5423–5428.

21 A. Fujishima, T. N. Rao and D. A. Tryk, *J. Photochem. Photobiol., C*, 2000, **1**, 1–21.

22 K. Ishibashi, A. Fujishima, T. Watanabe and K. Hashimoto, *J. Phys. Chem. B*, 2000, **104**, 4934–4938.

23 S. Kayano, K. Yoshihiko, H. Kazuhito and A. Fujishima, *Environ. Sci. Technol.*, 1998, **32**, 726–728.

24 Y. Ohko, A. T. Donald, K. Hashimoto and A. Fujishima, *J. Phys. Chem. B*, 1998, **102**, 2699–2704.

25 J. R. Li, C. H. Yang, L. G. Wu, Y. Q. Cao, T. Wang and B. Q. Jiang, *Colloids Surf., A*, 2015, **481**, 413–422.

26 S. X. Li, W. J. Liang, F. Y. Zheng, H. F. Zhou, X. F. Lin and J. B. Cai, *Sens. Actuators, B*, 2016, **224**, 48–54.

27 C. Guillard, E. Puzenat, H. Lachheb, A. Houas and J. M. Herrmann, *Int. J. Photoenergy*, 2005, **7**, 1–10.

28 Y. X. Li, Y. Xiang, S. Q. Peng, X. W. Wang and L. Zhou, *Electrochim. Acta*, 2013, **87**, 794–800.

29 Y. X. Li, F. He, S. Q. Peng, D. Gao, G. X. Lu and S. B. Li, *J. Mol. Catal. A: Chem.*, 2011, **341**, 71–76.

30 X. Jiang and T. Wang, *Environ. Sci. Technol.*, 2007, **41**, 4441–4446.

31 T. Wang, X. Jiang and J. Wang, *J. Colloid Interface Sci.*, 2010, **350**, 69–74.

32 T. Wang, L. Zhao, J. N. Shen, L. G. Wu and B. V. Bruggen, *Environ. Sci. Technol.*, 2015, **49**, 8004–8011.

33 A. J. Simamora, T. L. Hsiung, F. C. Chang, T. C. Yang, C. Y. Liao and H. P. Wang, *Int. J. Hydrogen Energy*, 2012, **37**, 13855–13858.

34 N. Yamada, M. Suzumura, F. Koiwa and N. Negishi, *Water Res.*, 2013, **47**, 2770–2776.

35 Y. Fiamegos, C. Stalikas and G. Pilidis, *Anal. Chim. Acta*, 2002, **467**, 105–114.

36 G. Norwitz, A. H. Bardsley and P. N. Keliher, *Anal. Chim. Acta*, 1981, **128**, 251–256.

37 M. Trillas, J. Peral and X. Domènech, *J. Chem. Technol. Biotechnol.*, 2015, **67**, 237–242.

38 E. Grabowska, J. Reszczyńska and A. Zaleska, *Water Res.*, 2012, **46**, 5453–5471.

39 Y. X. Li, F. He, S. Q. Peng, D. Gao, G. X. Lu and S. B. Li, *Int. J. Hydrogen Energy*, 2011, **36**, 10565–10573.

40 Y. X. Li, S. Y. Lin, S. Q. Peng, D. Gao, G. X. Lu and S. B. Li, *Int. J. Hydrogen Energy*, 2013, **38**, 15976–15984.

41 Y. X. Li, D. Gao, S. Q. Peng, G. X. Lu and S. B. Li, *Int. J. Hydrogen Energy*, 2011, **36**, 4291–4297.

42 L. Kong, C. H. Wang, H. Zheng, X. T. Zhang and Y. C. Liu, *J. Phys. Chem. C*, 2015, **119**, 16623–16632.

43 C. Xu, X. Wang and J. W. Zhu, *J. Phys. Chem. C*, 2008, **112**, 19841–19845.

44 G. Goncalves, P. A. A. P. Marques, C. M. Granadeiro, H. I. S. Nogueira, M. K. Singh and J. Grácio, *Chem. Mater.*, 2009, **21**, 4796–4802.

45 V. Loddo, G. MarcõÁ, C. MartõÂn, L. Palmisano, V. Rives and A. Sclafani, *Appl. Catal., B*, 1999, **20**, 29–45.

46 F. Dong, S. Guo, H. Q. Wang, X. F. Li and Z. B. Wu, *J. Phys. Chem. C*, 2011, **115**, 13285–13292.

47 Y. X. Li, H. Wang and S. Q. Peng, *J. Phys. Chem. C*, 2014, **118**, 19842–19848.

48 W. Y. Zhang, Y. X. Li and S. Q. Peng, *ACS Appl. Mater. Interfaces*, 2016, **8**, 15187–15195.

49 Y. X. Li, J. X. Wang, S. Q. Peng, G. X. Lu and S. B. Li, *Int. J. Hydrogen Energy*, 2010, **35**, 7116–7126.